# Regulating Oxygen Redox Reactions in Lithium-Rich Materials via $Al_2O_3$-Doped ZnO Layer for Enhanced Stability and Performance

Xinyu Cheng[1], Yuke Wang[1], Jia Lu[1], Wangqi Dai[1], Huanhao Lei[1], Jinning Zuo[1], Hong Li[2, *] and Zhengwen Fu[1, *]

[1] Shanghai Key Laboratory of Molecular Catalysts and Innovative Materials, Department of Chemistry, Fudan University, Shanghai, 200433, China.

[2] Institute of Physics, Chinese Academy of Sciences, Beijing, 100190, China.

[*] Corresponding author: zwfu@fudan.edu.cn (Zhengwen Fu); hli@iphy.ac.cn (Hong Li).

## 1. Experimental Section

### 1.1 Synthesis of Lithium-rich Material

Pristine $Li_{1.2}Ni_{0.133}Co_{0.133}Mn_{0.544}O_2$ (LRM) was synthesized using the Pechini method[1]. Lithium acetate, nickel acetate, cobalt acetate, and manganese acetate (AR, from Shanghai Hushi Laboratorial Equipment Co., LTD) in a molar ratio were added to water. To prevent lithium loss during high-temperature calcination, an additional 5% of lithium acetate was added. After dissolving, citric acid and ethylene glycol (AR, from Shanghai Hushi Laboratorial Equipment Co., LTD) were added. The molar ratio of metal salts to citric acid to ethylene glycol was 1:1:4. The mixture was heated and stirred at 80 °C until a gel was formed. The gel was dried in a vacuum oven at 120 °C for 12 hours, resulting in a sponge-like substance. This substance was ground and then calcined in a muffle furnace at 450 °C for 5 hours, followed by 900 °C for 12 hours, to finally obtain the lithium-rich material powder.

AZO-LRM and ZnO-LRM was prepared using magnetron sputtering with a target of 3% $Al_2O_3$-doped ZnO (AZO) and ZnO, respectively. The LRM powder was placed in a specially designed device and rolled, facing the sputtering target. The power was set to 300 W, with an $O_2$ : Ar = 1 : 3 gas mixture introduced, maintaining the chamber pressure at 0.4 Pa for sputtering. AZO-1, AZO-2, AZO-3 refer to samples sputtered for 1 hour, 2 hours and 3 hours, respectively. The sputtering rates of AZO and ZnO were measured by sputtering film onto silicon wafers, yielding rates of 10 and 8 nm/min, respectively. To match the coating thickness of AZO-2, the sputtering duration for ZnO-LRM was set to 2.5 hours.

### 1.2 Electrochemical Testing

The cathode active material, acetylene black, and PVDF were mixed uniformly in a ratio of 8: 1: 1 and then NMP was added to make a cathode slurry. After stirring for 10 hours, the slurry was evenly coated onto carbon-coated aluminum foil and dried at 80 °C for 12 hours to obtain cathode sheets. The electrode was cut into 12 mm diameter discs, with an active material content of approximately 5 mg. CR2032 half-cells were assembled in a glove box using an electrolyte of 1M $LiPF_6$ in EC: DMC = 1: 1 and

**Comment [Jaya]:** 序号,单位前面的空格

**Comment [Jaya]:** ZnO-LRM 的制备没写，下面的表征部分测试部分都没写

**Comment [Jaya]:** Al2O3

**Comment [Jaya]:** $O_2$: Ar = 1: 3

lithium metal as the anode. The cells were tested using a Neware Battery Test System. Before the long cycle test, they were activated by cycling twice at a 0.1 C. Except for high-temperature batteries, all other batteries were subjected to electrochemical testing at 25°C. All electrochemical data were obtained from multiple measurements. Electrochemical impedance spectroscopy (EIS) was measured using a Zennium pro electrochemical workstation (Zahner, Germany) with an amplitude of 5 mV over a frequency range from 100 kHz to 50 mHz. The galvanostatic intermittent titration technique (GITT) test involved 30 minutes of 0.1 C charge/discharge followed by 120 minutes of relaxation. The calculation formula for the lithium-ion diffusion coefficient is:

$$D_{Li+} = \frac{4}{\pi\tau}\left(\frac{R_s}{3}\right)^2\left(\frac{\Delta E_s}{\Delta E_t}\right)^2$$

where τ is the relaxation time (s), $\Delta E_s$ is the voltage change caused by the pulse (V), and $\Delta E_t$ is the voltage change during constant current charge/discharge (V). LRM is assumed to be a sphere with radius $R_s$ (cm). Differential electrochemical mass spectrometry (DEMS) was measured using a Linglu QMG220 from Shanghai. Before testing, Ar gas was introduced for 5 hours at a flow rate of 1 mL $min^{-1}$.

**1.3 Characterization**

The X-ray diffraction (XRD) patterns of LRM and AZO-LRM were measured using a Bruker D8 Advance diffractometer with Cu Kα radiation (λ = 1.5418 Å) in the 10-80° angle range. Scanning electron microscopy (SEM) and energy-dispersive X-ray spectroscopy (EDS) were conducted using a field-emission scanning electron microscope (FESEM, Hitachi Regulus 8100). Transmission electron microscopy (TEM) images were carried out on a JEOL JEM-ARM200F. X-ray photoelectron spectroscopy (XPS) was performed on a PHI 5000 Versaprobe III, with binding energies calibrated by C 1s (284.8 eV). Electron paramagnetic resonance (EPR) measurements were taken using a Bruker ESR5000.

**1.4 Density functional theory calculations**

**Comment [Jaya]:** 1

**Comment [Jaya]:** 用 calibrated by C 1s（284.8 eV）

**Comment [Jaya]:** ?

Density functional theory (DFT) calculations were performed using the Cambridge Sequential Total Energy Package (CASTEP) module in Materials Studio. The spin-polarized version of the Perdew-Burke-Ernzerhof (PBE) functional under the generalized gradient approximation (GGA) was adopted to treat the exchange correlation energy[2]. Due to the strongly correlated 3d-electrons, the rotationally invariant Dudarev method (DFT+U) was introduced, with the U value for Mn set to 3.9 eV according to previous literature[3]. Additionally, a kinetic energy cutoff of 520 eV for the plane wave basis and Brillouin zone integration on a grid with 3×2×1 were used. Geometric convergence tolerances were set for a maximum energy change of $10^{-5}$ eV per atom, a maximum force of 0.03 eV $Å^{-1}$, maximum stress of 0.05 GPa, and maximum displacement of 0.001 Å to ensure high accuracy. Density mixing electronic minimization was implemented, and the self-consistent field (SCF) tolerance was set to $10^{-6}$ eV per atom for energy convergence.

**Comment [Jaya]:** 全称+（DFT）

Comment [Jaya]: 图注好好改一下 不要有冒号 要有样品名字 放一句说

Comment [Jaya]: D e 空格

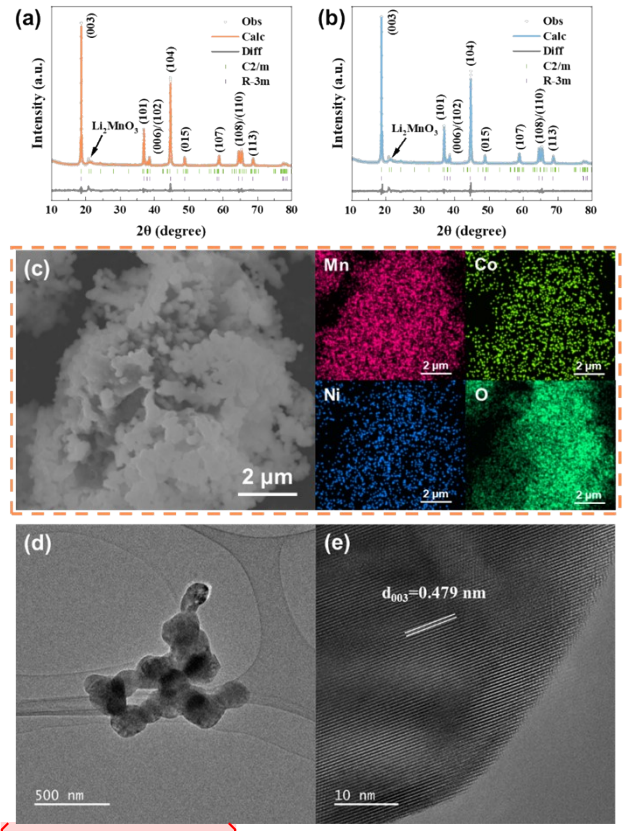


## 2. Supporting Figures and Tables

**Figure S1.** (a,b) XRD patterns and refinement results of (a) pristine LRM and (b) AZO-LRM. (c) SEM image and corresponding EDS elements mapping of pristine LRM. (d,e) TEM images of pristine LRM.

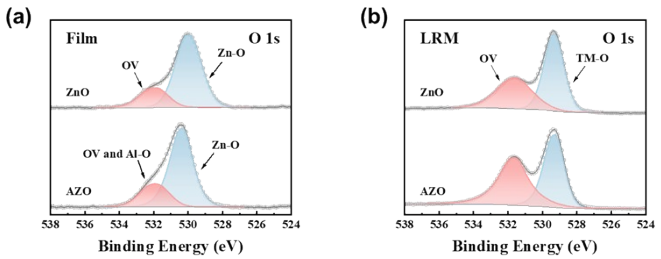


**Figure S2.** O 1s XPS spectra of (a) film and (b) coated LRM of AZO and ZnO.

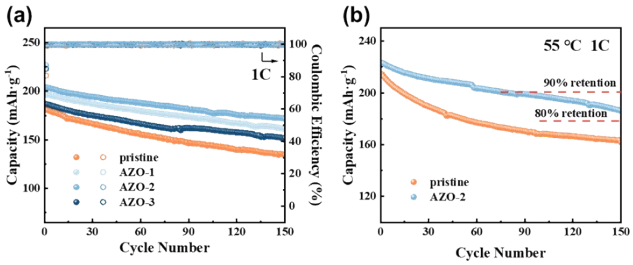


**Figure S3.** (a) Cycling performance of pristine LRM and three AZO-LRM at 1C. (b) Cycling performance of pristine LRM and AZO-2 at 1C under 55°C.

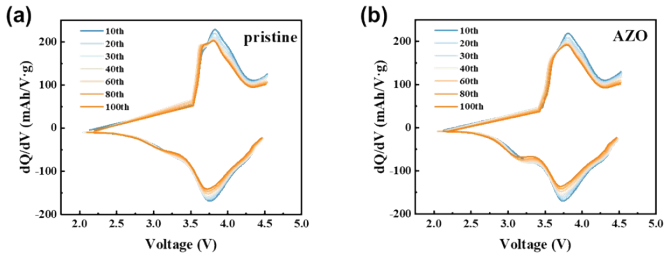


**Figure S4.** dQ/dV curves during cycling at 2.0-4.55V of (a) pristine LRM and (b) AZO-LRM.

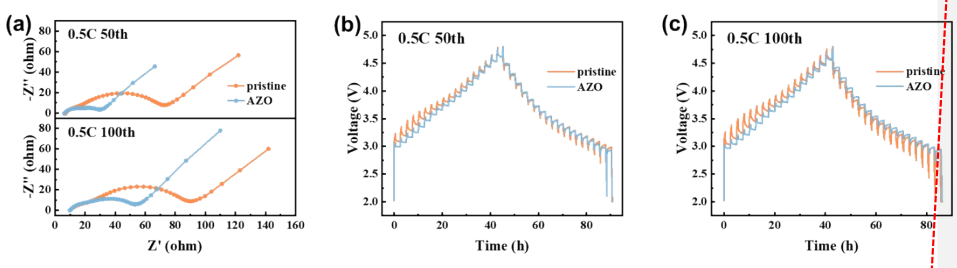


**Figure S5.** (a) EIS spectra of pristine LRM and AZO-LRM after 50 and 100 cycles at 0.5C. (b,c) Voltage-time curves of GITT of pristine LRM and AZO-LRM after (b) 50 cycles and (c) 100 cycles at 0.5C.

**Comment [Jaya]:** Of balabala

**Comment [Jaya]:** Of balaba

**Comment [Jaya]:** curves

**Comment [Jaya]:** 样品

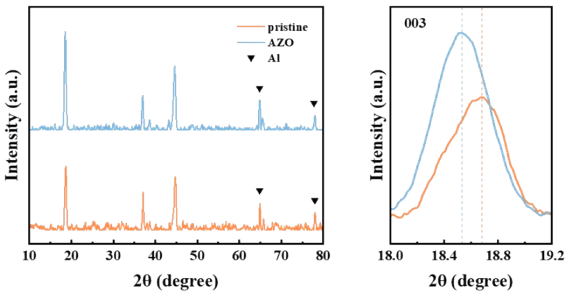


**Figure S6.** The XRD patterns and magnified images of the 003 diffraction peaks for pristine LRM and AZO-LRM after the first charging cycle.

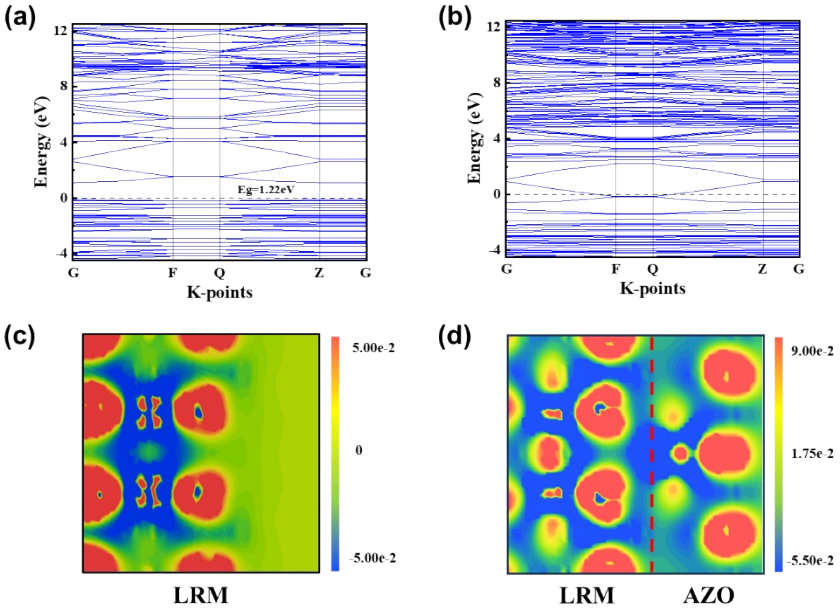


**Figure S7.** (a,b) Interface band structure of (a) pristine LRM surface and (b) AZO-LRM interface. (c,d) Differential charge density of (c) pristine LRM surface and (d) AZO-LRM interface.

Comment [Jaya]: 3 点 能带箭头 图注反场箭头

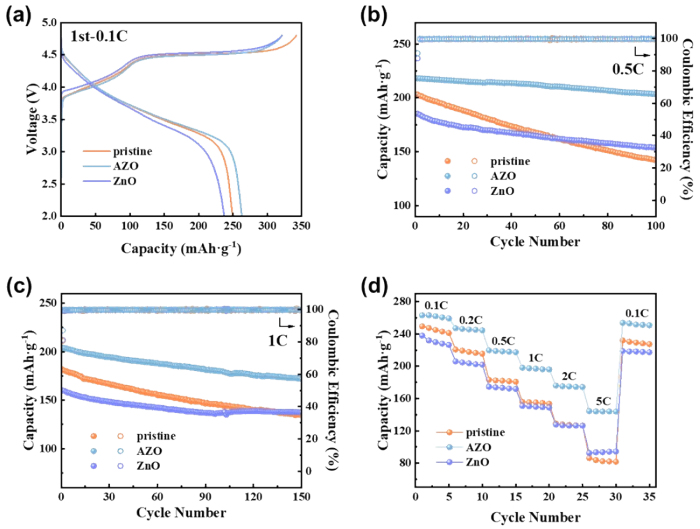


**Figure S8.** (a) Voltage-capacity curves of pristine LRM, AZO-LRM and ZnO-LRM. for initial charge-discharge at 0.1C. Cycling performance at (b) 0.5C and (c) 1C and (d) rate capability of pristine LRM, AZO-LRM and ZnO-LRM.

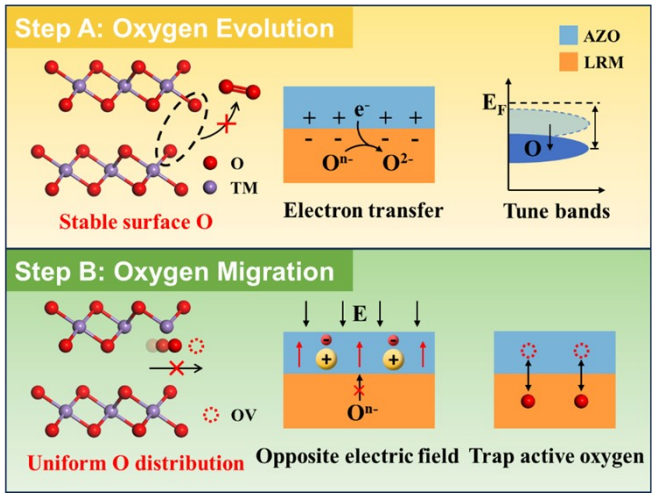


**Figure S9.** The mechanism of AZO inhibition of oxygen evolution and oxygen migration.

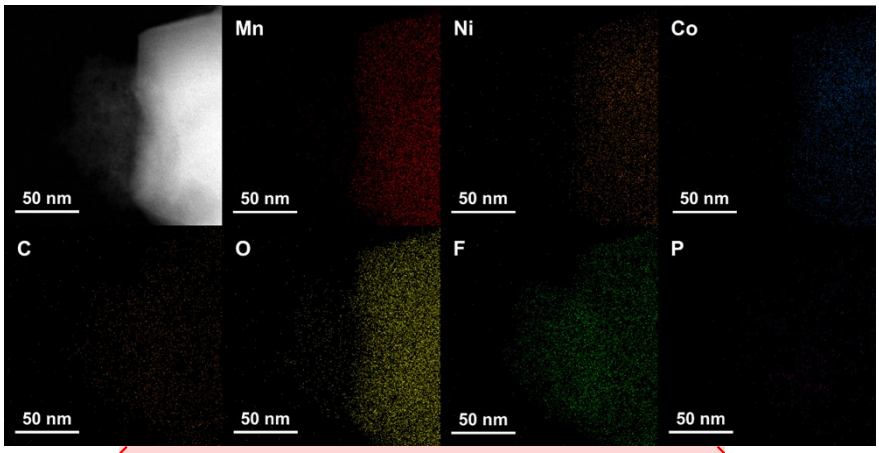


**Figure S10.** TEM-EDS images and corresponding elemental mapping of pristine LRM after cycling.

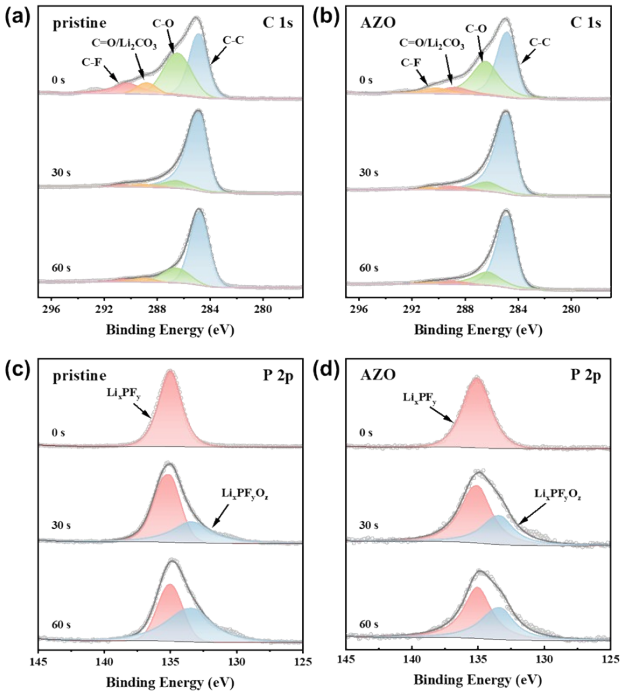


**Figure S11.** XPS spectra at different etching depths of the cycled electrode surfaces. C 1s spectra for (a) pristine LRM and (b) AZO-LRM, and P 2p spectra for (c) pristine LRM and (d) AZO-LRM.

**Comment [Jaya]:** ？

**Comment [Jaya]:** 两端对齐

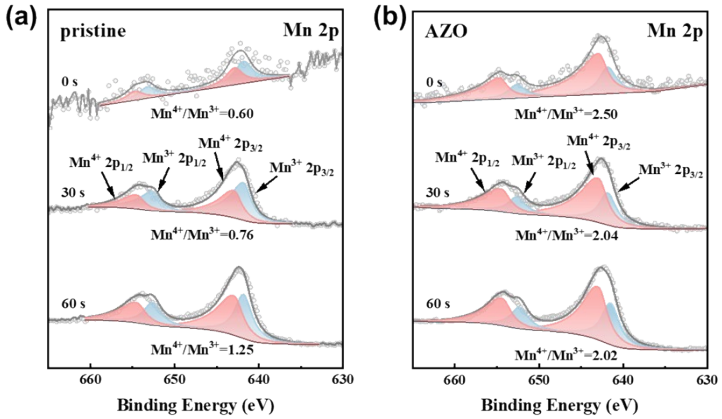


**Figure S12.** Mn 2p XPS spectra of (a) pristine LRM and (b) AZO-LRM at different etching depths.

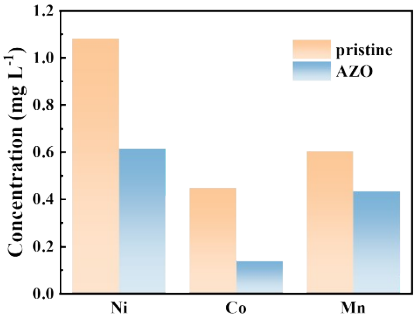


**Figure S13.** The concentration of transition metal ions in the electrolyte after cycling for pristine LRM and AZO-LRM.

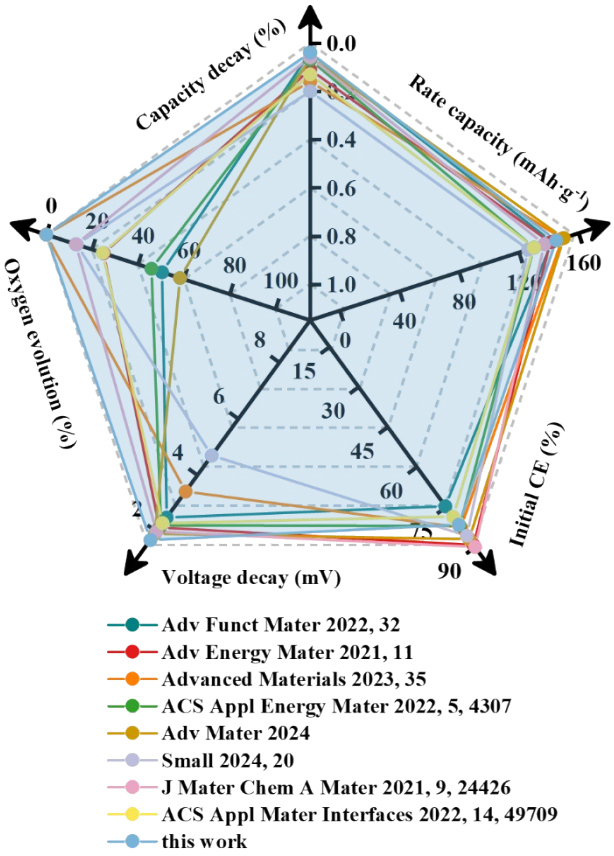


**Figure S14.** Comparison of electrochemical performance with other literature.

**Table S1.** XRD refinement result of pristine LRM and AZO-LRM.

Comment [Jaya]: 表格不能放图片

| | a (Å) | c (Å) | c/a | V (Å$^3$) | $I_{(003)}/I_{(104)}$ |
|---|---|---|---|---|---|
| **pristine** | 2.84979 | 14.22145 | 4.99035 | 100.023 | 1.611 |
| **AZO** | 2.84989 | 14.22223 | 4.99045 | 100.036 | 1.573 |

**Table S2.** Element content measured by ICP-OES of pristine LRM and AZO-LRM.

| | Li (%) | Ni (%) | Co (%) | Mn (%) | Zn (ppm) | Al (ppm) |
|---|---|---|---|---|---|---|
| **pristine** | 10.50 | 10.32 | 10.35 | 38.76 | 30.84 | 3.37 |
| **AZO** | 10.55 | 10.11 | 10.25 | 38.79 | 6804.21 | 82.20 |

**Table S3.** EIS fitting result of pristine LRM and AZO-LRM.

| | | $R_{CEI}$ (Ω) | $R_{ct}$ (Ω) | $R_D$ (Ω) |
|---|---|---|---|---|
| **50$^{th}$** | **pristine** | 21.0 | 6.8 | 70.3 |
| | **AZO** | 4.2 | 4.1 | 57.9 |
| **100$^{th}$** | **pristine** | 25.3 | 7.0 | 74.6 |
| | **AZO** | 13.5 | 6.0 | 64.2 |

**Table S4.** Comparison of the strategy and mechanism in inhibiting oxygen release with other literature.

Comment [Jaya]: Reference 右边

| Strategy | Mechanism | Reference |
|---|---|---|
| Oxygen scavenger polymer coating | Scavenger reactive oxygen species | 4 |
| N-doped graphene wrapping | Trap active oxygen species | 5 |
| Carbon-rock salt/spinel composite coating | Surface reconstruction | 6 |
| Nb/Al surface doping, OV creating and $Al_2O_3$ coating | Strong Nb-O bonds and surface OV suppress gas release | 7 |
| Oxygen deficient perovskite coating | Capture oxygen moieties | 8 |
| Amorphous $Co_xB$ coating | Lower energy of O 2p state | 9 |
| Ce doping and $Li_2CeO_3$ coating | Pseudo-bonding effect and self-build-in electric field | 10 |
| Inverse spinel $Mg_2TiO_4$ coating | Dielectric polarization coating creates reverse electric field | 11 |
| Spinel phase and $Li_3PO_4$ coating | Spinel phase reduce O 2p band | 12 |
| $Al_2O_3$-doping ZnO coating | CCL constructing an internal self-built electric field<br>SCL lowing energy of O 2p state<br>Trap active oxygen species | This work |

Reference


1 J. Chen, Z. Huang, W. Zeng, J. Ma, F. Cao, T. Wang, W. Tian and S. Mu, *ACS Appl Mater Interfaces*, 2022, **14**, 6649–6657.

2 G. Sun, F. Da Yu, L. F. Que, L. Deng, M. J. Wang, Y. S. Jiang, G. Shao and Z. B. Wang, *Nano Energy*, DOI:10.1016/j.nanoen.2019.104102.

3 Y. Liu, H. Zhu, H. Zhu, Y. Ren, Y. Zhu, Y. Huang, L. Dai, S. Dou, J. Xu, C. J. Sun, X. L. Wang, Y. Deng, Q. Yuan, X. Liu, J. Wu, Y. Chen and Q. Liu, *Adv Energy Mater*, DOI:10.1002/aenm.202003479.

4 S. Y. Kim, C. S. Park, S. Hosseini, J. Lampert, Y. J. Kim and L. F. Nazar, *Adv Energy Mater*, DOI:10.1002/aenm.202100552.

5 M. Chen, G. Zhang, B. Wu, M. Liu, J. Chen, W. Xiang and W. Li, *ACS Appl Energy Mater*, 2022, **5**, 4307–4317.

6 Y. Ye, S. Yuan, S. Zhang, T. Liu, J. Wang and Q. Wang, *Small*, DOI:10.1002/smll.202307669.

7 Z. Shi, Q. Gu, L. Yun, Z. Wei, D. Hu, B. Qiu, G. Z. Chen and Z. Liu, *J Mater Chem A Mater*, 2021, **9**, 24426–24437.

8 Y. Lei, Y. Elias, Y. Han, D. Xiao, J. Lu, J. Ni, Y. Zhang, C. Zhang, D. Aurbach and Q. Xiao, *ACS Appl Mater Interfaces*, 2022, **14**, 49709–49718.

9 J. Chen, H. Chen, Y. Mei, J. Gao, A. Dai, Y. Tian, W. Deng, G. Zou, H. Hou, C. E. Banks, T. Liu, K. Amine and X. Ji, *Energy Storage Mater*, 2022, **52**, 736–745.

10 J. Chen, G. Zou, W. Deng, Z. Huang, X. Gao, C. Liu, S. Yin, H. Liu, X. Deng, Y. Tian, J. Li, C. Wang, D. Wang, H. Wu, L. Yang, H. Hou and X. Ji, *Adv Funct Mater*, DOI:10.1002/adfm.202004302.

11 W. Zhang, Y. Sun, H. Deng, J. Ma, Y. Zeng, Z. Zhu, Z. Lv, H. Xia, X. Ge, S. Cao, Y. Xiao, S. Xi, Y. Du, A. Cao and X. Chen, *Advanced Materials*, DOI:10.1002/adma.202000496.

12 Q. Jiang, X. Li, Y. Hao, J. Zuo, R. Duan, J. Li, G. Cao, J. Wang, J. Wang, M. Li, X. Yang, M. Li, W. Li, Y. Xi, J. Zhang and W. Xiao, *Adv Funct Mater*, DOI:10.1002/adfm.202400670.